PROCEEDINGS OF SPIE

SPIEDigitalLibrary.org/conference-proceedings-of-spie

Observations of quasar host galaxies with laser guide star AO

Elinor L. Gates, Mark Lacy, Willem de Vries

Elinor L. Gates, Mark Lacy, Willem de Vries, "Observations of quasar host galaxies with laser guide star AO," Proc. SPIE 5490, Advancements in Adaptive Optics, (25 October 2004); doi: 10.1117/12.552078

SPIE.

Event: SPIE Astronomical Telescopes + Instrumentation, 2004, Glasgow, United Kingdom

Observations of quasar host galaxies with laser guide star AO

Elinor L. Gates[a], Mark Lacy[b], and Wim de Vries[c,d]

[a]University of California Observatories/Lick Observatory, P.O. Box 85, Mount Hamilton, CA, USA 95140;
[b]Spitzer Science Center, California Institute of Technology, 1200 E. California Boulevard, Pasadena, CA USA 91125;
[c]University of California, One Shields Ave, Davis, CA USA 95616;
[d]Lawrence Livermore National Laboratory, L-413, 7000 East Ave, Livermore, CA USA 94550

ABSTRACT

We report on observations of two quasar host galaxies made with the Lick Observatory adaptive optic system using a laser guide star tuned to the wavelength of the sodium D lines. A brief outline of the system is given, and a description of its performance when obtaining science data. We discuss techniques for obtaining calibration of the point spread function and the analysis steps required to obtain useful scientific results. We present H-band images of quasar host galaxies made with the system. Estimates of the host galaxy magnitudes and central black hole masses were made from these data. These are the first observations of quasar host galaxies with a sodium laser guide star.

Keywords: Laser guide stars, quasar host galaxies

1. INTRODUCTION

Detection of the faint host galaxies of bright quasars has been a long-standing problem in observational extra-galactic astronomy. Although the host galaxy and the bright, unresolved quasar nucleus typically have similar total fluxes, the diffuse nature of the galaxy emission can frequently be confused with the extended wings of a poorly-characterized PSF. Cosmological surface brightness dimming by a factor of $(1+z)^4$, where z is the redshift, makes detecting the host galaxies of high redshift quasars particularly challenging. Initial attempts at host galaxy detection using photographic plates were successful in only finding the hosts of nearby relatively faint quasars.[1,2] Application of digital scanning technology to photographic plates allowed the first attempts at PSF subtraction,[3] pushing host detections to redshifts, $z \sim 0.5$, and allowing quantitative estimates of host galaxy magnitudes. The advent of digital, linear CCD detectors made modeling of the contribution of the PSF easier (e.g., Smith et al.[4]). The real breakthroughs in quasar host studies came with the advent of HST, with its small, more stable PSF, and near-infrared array detectors. Early HST studies with the optical instruments on board allowed the detailed study of nearby quasar hosts.[5,6] In parallel, ground-based studies in the near-infrared were able to study the quasars at wavelengths where the flux of the quasar was minimized with respect to the flux of the host galaxy.[7] The marriage of HST's PSF and the near-infrared NICMOS detector allowed routine discoveries of quasar hosts up to $z \sim 2$.[8,9]

Adaptive optics are a relatively recent addition to the available techniques for quasar host imaging. Although problematic in some respects (principally PSF variability) AO offers the ability to study larger samples than are practical with the limited observing time available with HST, and, through using 10 m-class telescopes, better resolution and surface brightness sensitivity (e.g., Stockton, Canalizo and Close,[10] Lacy et al.,[11] Croom et al.[12]). Although it is important to bear in mind that surface brightness sensitivity is fundamental to the detection of quasar hosts (for example, with a warm deformable mirror, observing in H-band is usually superior to K-band due to the lower background, even though the PSF is poorer), AO does significantly improve the ability to detect hosts through concentrating the quasar light into the center of the galaxy image, thus improving contrast between the quasar PSF and the extended galaxy.

Send correspondence to: E.L.G.: egates@ucolick.org; 1 831 459 5910

Advancements in Adaptive Optics, edited by Domenico Bonaccini Calia, Brent L. Ellerbroek, Roberto Ragazzoni, Proceedings of SPIE Vol. 5490 (SPIE, Bellingham, WA, 2004)
0277-786X/04/$15 · doi: 10.1117/12.552078

In parallel with the development of the techniques for observing quasar hosts the scientific reasons for observing them have also evolved. Initially, observations were seen as an aid in understanding the nature of quasars themselves, to help determine whether their redshifts were cosmological in origin. Later, the triggering mechanism for quasars was the principal interest when several quasars were found to have interacting host galaxies (e.g. Stockton and MacKenty[13]). In recent years, the discovery that the (now mostly dormant) black holes in the nuclei of nearby galaxies have masses which correlate with the luminosity and velocity dispersion of their host galaxies has directly linked the quasar phenomenon to galaxy evolution. Black hole mass estimates from host galaxy luminosities can be compared to those which use the results of reverberation mapping and the widths of broad emission lines, with generally consistent results.[14,15] This gives us the possibility of understanding the black hole mass–galaxy mass correlation through a study of the evolution of quasar hosts.

Reliable black hole mass estimates have also stimulated long-standing debates on how the observational properties of quasars, such as their emission-line spectra, radio-loudness and accretion rates may (or may not) depend on black hole mass.[16–20] Recent work on the relationship between starbursts and active galactic nuclei using results from the Sloan Digital Sky Survey (SDSS)[21] have reinvigorated studies on the links between quasar activity, starbursts and galaxy mergers.

One problem that has bedeviled quasar astronomy throughout its history is that selection of quasar samples has been somewhat haphazard. Optical and X-ray selection techniques are only sensitive to quasars with little dust or gas in the host galaxy to redden or absorb the quasar light. Radio selection is not sensitive to reddening, but only $\sim 10\%$ of quasars are bright radio emitters, and the selection effects associated with radio quasar samples are only just beginning to be understood. The advent of the SDSS quasar sample has been a large step forward in this respect as, by selecting candidate quasars on the basis of having colors inconsistent with them being stars, rather than simply being very blue, they are able to pick objects that would be missed from traditional quasar surveys.[22,23] We picked the SDSS quasar sample as the basis for our adaptive optics study in the hope that it would give us a better understanding of the quasar population rather than the samples previously studied by HST, which were typically selected either on the basis of being very blue, bright in the X-ray, or bright in the radio, and therefore may not be representative of the quasar population as a whole.

2. LICK OBSERVATORY LGS-AO SYSTEM

Data were acquired using the laser guide star (LGS) AO system on the 3-m Shane Telescope at Lick Observatory. The natural guide star (NGS) AO instrument has been in routine scientific use by the University of California observing community since 2000 and the LGS system has been available since 2002. The AO system is located at the Cassegrain focus of the telescope, has 40 subapertures, uses a Shack-Hartmann wavefront sensor (WFS), and a 61 actuator deformable mirror. An upgrade to the real-time control computer during 2003 allows the system to operate at up to 1 kHz rates. In LGS mode an avalanche photodiode (APD) quadcell is used to measure tip-tilt from an $m_V < 16$ natural guide star within $55''$ of the science target. Observing efficiency in LGS mode is now approaching the observing efficiency of NGS for brighter ($m_V < 15$) tip-tilt stars. LGS efficiency and performance continues to improve through upgrades to the motor control software and hardware to compensate for system flexure and real-time control computer software upgrades.

An artificial star is created by a laser tuned to the 589 nm resonance line of atomic sodium, which is present in the atmosphere at about 90 km altitude. The laser beacon is generated by four frequency doubled ND:YAG lasers pumping a dye laser. The 589 nm seed beam for the dye amplifier is created by a dye master oscillator grating and etalon system. The laser pulse rate is 15 kHz and pulse width is 150 ns. The laser launch telescope is mounted on the side of the the Shane telescope and aligned so that the artificial star is on the telescope optical axis and aligned with the same WFS as used in NGS observations. During LGS operations a mirror in front of the WFS is swapped for a dichroic beamsplitter that sends $\lambda < 600$ nm light to the WFS and $600 < \lambda < 1000$ nm light to the APD tip-tilt sensor. The sodium laser power is typically 12 W, corresponding to an $m_V \sim 9$ star and produces a spot size of approximately $2\farcs2$ FWHM at the sodium layer. Spot elongation is insignificant because the launch telescope is only 1.5 m from the telescope optical axis. The WFS is on a moving stage that can track changes in the height of the sodium layer with airmass. A low-bandwidth Hartmann WFS is used to monitor the height of the sodium layer and adjust positioning of the primary WFS. An FAA safety agreement limits LGS propagation to between 11 pm and 5 am and to zenith distances less than 45 degrees because of

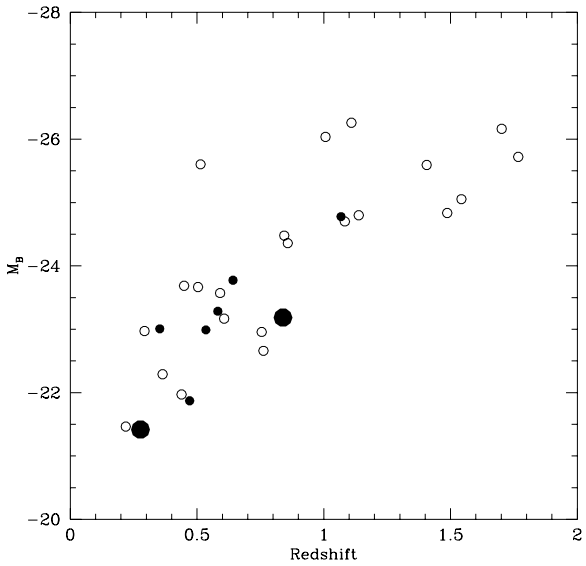

Figure 1. Absolute magnitude versus redshift for the quasars observed so far. Closed symbols show objects observed using the laser guide star, open symbols those observed with a natural guide star. The two quasars whose analysis is discussed in this paper are shown as the large closed symbols. Note that the magnitude limit of the SDSS sample is responsible for the apparent correlation of absolute magnitude with redshift.

Lick Observatory's close proximity to a number of large international airports. The Lick AO system is further described in Bauman et al.[24, 25] and Gavel et al.[26–28]

The AO system feeds IRCAL, a near-infrared (NIR) camera containing a PICNIC HgCdTe 256x256 array.[29] The $f/28$ output of the AO system gives a plate scale of $0\farcs076$/pixel and a field of view of $19\farcs4$ x $19\farcs4$. The diffraction limited point spread function (PSF) is Nyquist sampled at K band (2.2 μm) with this plate scale. The camera contains cold aperture and filter wheels populated with typical NIR broadband filters, a selection of narrowband filters, H- and K-grisms, slits, occulting finger, and a Wollaston prism,[30] enabling a wide range of imaging, spectroscopic, and polarimetric capabilities. A warm filter wheel can be placed in front of the IR camera to accommodate additional filters if necessary.

3. SAMPLE SELECTION

Quasars were selected from the SDSS EDR and DR1 releases.[23, 31] We used the USNO and HST Guide Star catalogs to find quasars with guide stars within $45''$. Targets for adaptive optics imaging using the Natural Guide Star (NGS) mode were selected to have guide stars brighter than $R \approx 12$. For the Laser Guide Star mode, we selected objects with tip-tilt guide stars brighter than $R \approx 15$. About 1% of the of the 16,700 SDSS DR1 quasars have a suitable NGS guide star within $35''$, and about 8% have a suitable LGS guide star within $35''$. We imposed a magnitude limit of $r = 20$ to ensure that the quasars were well-detected on individual 300 s exposures in H band so that images could be accurately centroided in individual frames. We also imposed an upper redshift limit of $z = 1.8$, beyond which surface brightness dimming makes detection of faint quasar hosts difficult using only a 3-m telescope. The absolute magnitude versus redshift for all the quasars in our sample is displayed in Figure 1.

4. DATA ACQUISITION

Successful observations of quasar hosts requires both a small PSF and surface brightness sensitivity. The 3-m Shane Telescope and both the NGS and LGS AO systems were used for data acquisition. While the best AO

performance for the Lick system is at K band, the thermal background from warm instrument optics makes it desirable to use H band to get a higher signal-to-noise ratio on the low surface brightness host galaxy emission.

Our observational strategy was a compromise between low overheads and reliable PSF monitoring. Observations of each quasar were interspersed with observations of the quasar guide star (QGS) approximately every 50 minutes. A single observation of a PSF star–PSF guide star (PGS) pair was made for each quasar. The selected PSF star was at the same distance and position angle from its guide star as the quasar was from its guide star. The PSF star observation was used to calibrate the effect of going off-axis.

Our first successful attempt to obtain science-quality data on quasar hosts occurred on 2002 September 22 (UT). Two quasars from the LGS sample were observed, SDSS 2324+0021 ($z = 0.28$) and SDSS 0244+0028 ($z = 0.84$). Details of the quasars are given in Table 1, and they are shown as the large symbols in Figure 1. Observations of further quasars with the LGS system have been made (shown by small closed symbols in Figure 1), but the data have yet to be analyzed. Our first three NGS quasar host observations appeared in Lacy et al..[11] Table 2 lists the details of the guide stars for these two quasars, and Table 3 lists the PSF stars and their guide stars.

The data were taken as several five-point dither position mosaics, each pointing lasting 5 minutes. Small offsets of $1''$–$2''$ were made between each mosaic. Total integration times were 55 minutes for SDSS 2324+0021 and 125 minutes for SDSS 0244+0028. The QGS observations were made using the same five-point mosaic with integration times of 10 s per pointing. The PSF stars were also observed using the five-point grid with exposures times of 2–3 s per point. Flux calibration was achieved using standard stars P533-D and P138-C.[32] The natural seeing was $\sim 0\farcs9$ in H band. AO corrections were made at 200 Hz for SDSS 2324+0021 and 100 Hz for SDSS 0244+0028. The slower AO correction rate for SDSS 0244+0028 was necessary because the laser spot size increased and also decreased in brightness. This was caused by SDSS 0244+0028 being observed at a higher airmass than SDSS 2324+0021. It did not significantly change the image quality of the data, as the FWHM of the QGS for both quasars were comparable (see Table 4). Images of the fields are shown in Figure 2.

Table 1. Quasar Targets

Quasar	RA (J2000.0)	Dec (J2000.0)	r_{AB}	z
SDSS 2324+0021	23 24 08.4	+00 21 19	18.8	0.28
SDSS 0244+0028	02 44 48.9	+00 28 59	19.7	0.84

Table 2. Quasar Guide Stars

Quasar	QGS RA (J2000.0)	QGS Dec (J2000.0)	QGS m_R	Separation (arcsec)	P.A. (degrees)
SDSS 2324+0021	23 24 10.0	+00 21 43	14.1	34	46
SDSS 0244+0028	02 44 47.8	+00 29 28	13.3	34	330

5. DATA ANALYSIS AND PSF CALIBRATION

Following dark subtraction and flat fielding, the quasar data were combined using the DIMSUM package in IRAF*.

*IRAF is distributed by the National Optical Astronomy Observatory, which is operated by the Association of Universities for Research in Astronomy, Inc., under cooperative agreement with the National Science Foundation.

Table 3. PSF Stars and PSF Guide Stars

Quasar	PSF m_R	RA (J2000.0)	Dec (J2000.0)	PGS m_R	Separation (arcsec)	P.A. (degrees)
SDSS 2324+0021	11.8	23 26 55.8	+00 04 46	13.6	36	52
SDSS 0244+0028	15.5	02 45 45.4	+00 11 31	13.9	33	325

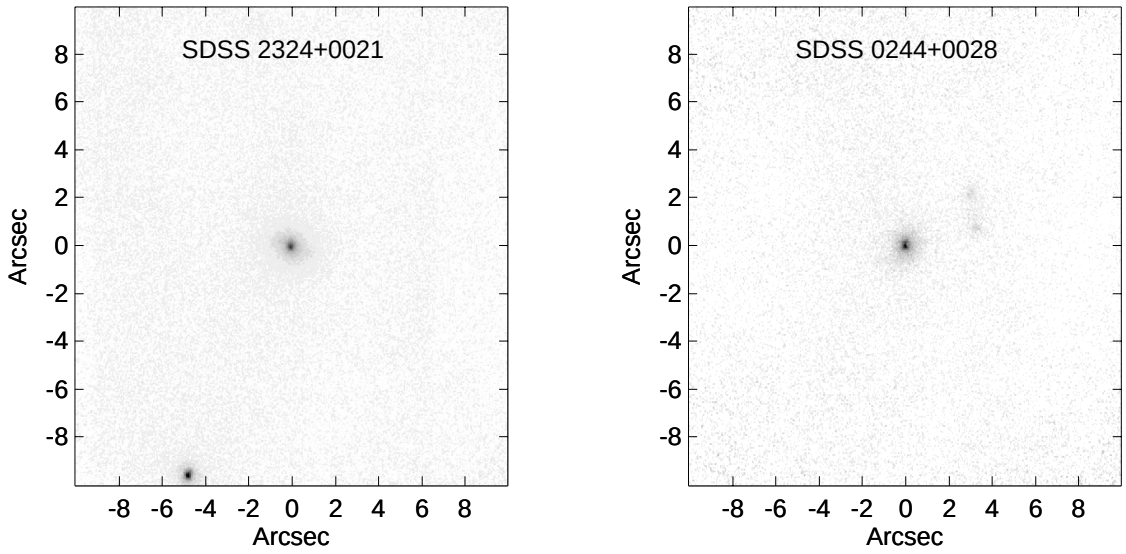

Figure 2. Left: AO corrected field of SDSS 2324+0021. A foreground star is visible approximately 10″ to the southeast of the quasar. Right: AO corrected field of SDSS 0244+0028. Two additional faint galaxies are visible within a few arcseconds of the quasar. North is up and east is to the left.

The key to analyzing these data is the AO PSF, which is both variable in time and dependent on many observing parameters. The brightness and color of the natural guide star (which determines the accuracy of the tip-tilt correction), the spot size and brightness of the LGS (which determines the accuracy of the AO correction), and the color of the PGS compared to the QGS can influence the size and shape of the PSF. Ideally, quasar observations would be interleaved with frequent sampling of the off-axis PSF, using observations of a nearby PSF star–PGS pair well matched in guide star brightness, color, separation and position angle to the quasar–QGS pair. However, to produce a more efficient procedure, we used the technique described in Section 4 and later attempted to reconstruct the PSF from frequent observations of the guide star and a single observation of a PSF star–PGS pair chosen for proximity to the quasar rather than exact matches in color and brightness to the quasar–QGS pair. The procedure, as described below, enables us to synthesize a PSF with a FWHM close to that of the quasar observations, even if the QGS and PGS have slightly different brightnesses and therefore AO corrections that differ in quality. It also enables us to remove any component of the aberration due to anisoplanatism effects, which are constant in time. Steinbring et al.[33] show that a similar strategy of determining a kernel map for the off-axis variation of the PSF by observing a crowded stellar field can be effective, and remove the bulk of the anisoplanatism effects on the PSF.

The first step of the PSF synthesis procedure is to deconvolve the PSF star by the PGS. We used the Lucy deconvolution algorithm and enough iterations were performed to reduce the FWHM of the PSF star to significantly less than that of the PGS. Care was taken to stop the deconvolution process before artifacts appeared in the deconvolved image. This produces an "off-axis kernel."

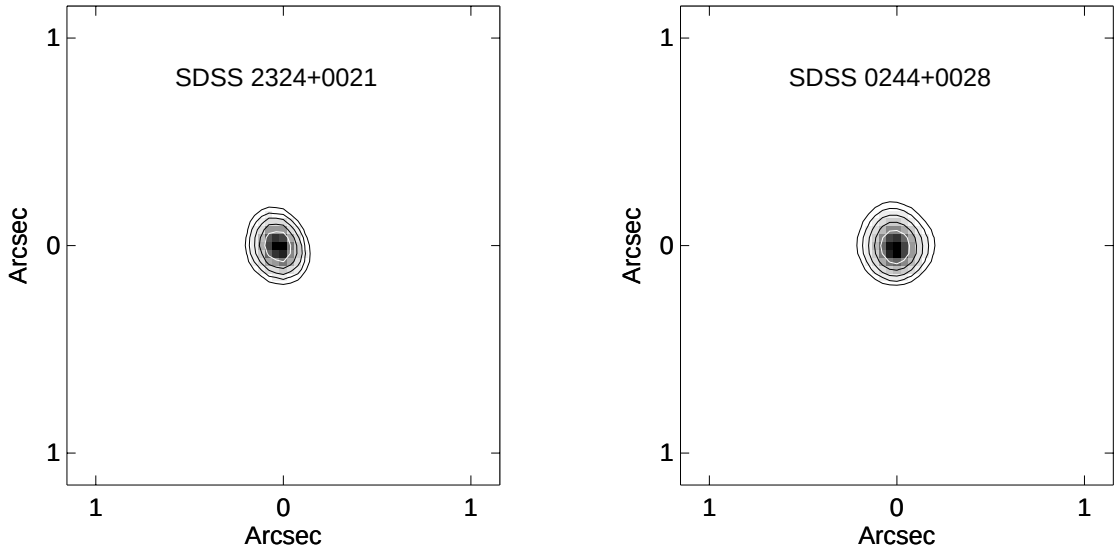

Figure 3. Off-axis kernels for each of the quasar observations, obtained by deconvolving the PSF star by the PGS observations. This kernel is convolved with the QGS observations to synthesize the observed PSF. The contours are logarithmic, spaced by factors of two, overplotted on a linear gray-scale stretch.

The off-axis kernel is then convolved with the average on-axis QGS observations to make the synthesized PSF. This process minimizes problems of a mismatch between the QGS and PGS brightness and color.

While this procedure was developed and tested for NGS observations,[11] it is also applicable to LGS observations because of the natural off-axis tip-tilt star, even though anisoplanatism effects are minimized due to the LGS always being on axis. In using this technique in NGS mode, we saw a characteristic elongation of the PSF kernel along the axis aligned with vector joining the PSF to its guide star. This elongation is not seen in the LGS PSF observations, presumably because all high order corrections are on axis and the only off-axis errors are from residual tip-tilt errors. Figure 3 shows the off-axis PSF kernels for both observed quasars.

Because the diffraction limited PSF is undersampled at H Band, the image quality was assessed by measuring the Gaussian FWHM rather than the Strehl ratio. Table 4 summarizes the FWHMs of the QGS, PGS, and PSF star for each observed quasar.

Table 4. Image Quality

Quasar	Raw QSO FWHM (arcsec)	Synth. PSF FWHM (arcsec)	QGS FWHM (arcsec)	PSF Star FWHM (arcsec)	PGS FWHM (arcsec)
SDSS 2324+0021	0.39	0.32	0.23	0.30	0.22
SDSS 0244+0028	0.33	0.39	0.24	0.33	0.31

6. HOST GALAXY DETECTION AND PROPERTIES

6.1. Modeling the Host Galaxies

The host galaxies were modeled according to the method outlined by McLure, Dunlop, and Kukula[34] by fitting PSF plus galaxy model profiles (convolved by the PSF) and minimizing χ^2.

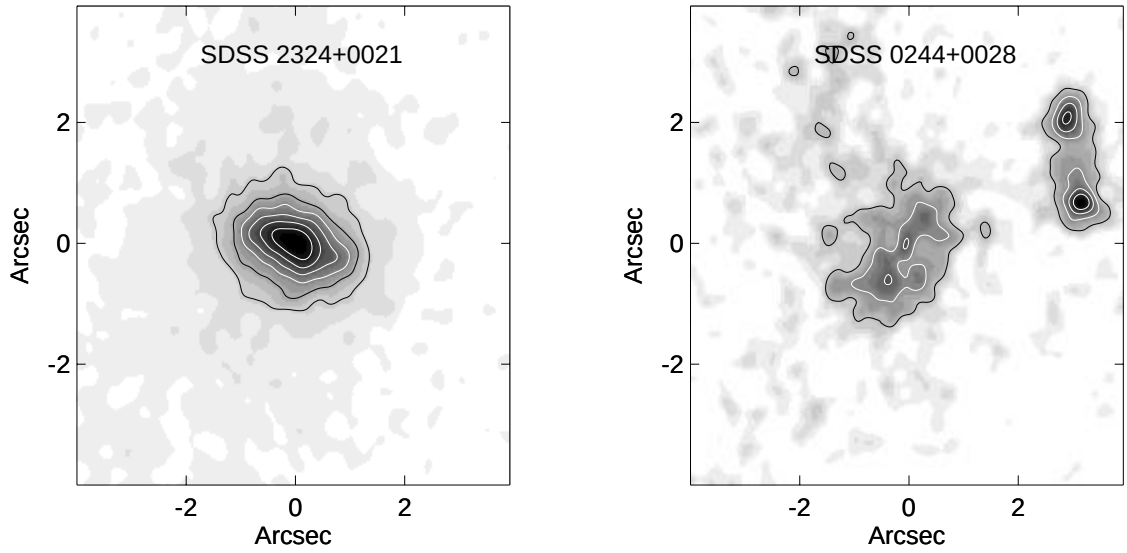

Figure 4. Host galaxies after subtraction of the best fit PSF model of the quasar nucleus. Images were smoothed by a 0.″27 FWHM Gaussian. North is up and east is to the left.

Initial host magnitudes and scale sizes were determined by subtracting the PSF so that the residual was roughly flat in the center of the quasar within radius r_{in} and declined monotonically outside r_{in}. r_{in} was chosen such that outside this radius the PSF residuals were small compared with the noise in the images. The resulting image was smoothed and fit using the ELLIPSE routine in IRAF to provide an estimate of the host major axis position angle and axial ratio. This technique provides galaxy parameters that are model independent and a reasonable starting point for full modeling.

We fitted the scale size, flux, major axis position angle, and axial ratio of the host galaxy model and the flux and position of the nucleus. The galaxy and quasar centers were constrained to be the same. Also, small adjustments in the background subtraction were made to set the residual to zero at large radii ($r > 3''$). Figure 4 shows the host galaxies after subtraction of the best fit PSF corresponding to the quasar nucleus. Both elliptical and disk galaxy models were tried, but neither was a significantly better fit to the data. Results of the modeling are listed in Table 5. We used NFIT1D within IRAF to fit one-dimensional exponential disk and elliptical profiles to the host galaxy radial profiles. The host radial profiles were determined using the RADPROF procedure in IRAF on the host after the best two-dimensional PSF fit to the quasar core was subtracted. The SDSS 2324+0021 host radial profile is clearly better fit by the exponential disk model than the elliptical model, as shown in Figure 5. One-dimensional modeling of the SDSS 0244+0028 host favored the elliptical galaxy profile, but PSF fitting errors of the quasar nucleus dominated the inner region of the host radial profile and the field galaxies caused confusion at large radii for the fits. The one-dimensional profile is difficult to fit unambiguously for fainter hosts because the amount of point-source nuclear emission is degenerate with the inner part of the host profile, which is where most of the information on the profile shape is.

Errors in the magnitudes of the hosts were estimated by combining errors from noise, systematics from PSF mismatch, and photometric errors. Errors in the magnitudes and scale sizes due to noise in the χ^2 fitting were estimated by randomly shuffling the pixel values in the residual image, adding back the model, and refitting with a starting vector randomly changed by 10% in each fitted paramter (PSF scale, galaxy flux, half-light radius, axial ratio, and position angle) from the best fitting parameter set.

In the case of SDSS 0244+0028 the synthesized PSF had a FWHM that was wider than either the PSF star or the quasar due to both the large PGS FWHM and as yet undetermined deconvolution errors. In this case we

Table 5. Observed Host Galaxy Properties

Quasar	m_e	m_d	Δm	θ_e	θ_d	$\Delta\theta$	χ^2_e/dof	χ^2_d/dof	AR_e	AR_d	PA_e	PA_d
SDSS 2324+0021	16.5	16.8	0.1	0.43	0.50	0.1	1.05	1.03	2.2	1.9	71	72
SDSS 0244+0028	17.3	17.5	0.1	0.80	0.81	0.4	0.57	0.57	2.3	1.0	154	0

Notes: m_e is the magnitude of the best-fitting elliptical galaxy model, and m_d is the best-fitting disk galaxy model. All magnitudes are H-band, Vega magnitudes and are measured in square apertures $7''.5$ on a side centered on the quasar. Δm is the estimated error in the magnitudes (both systematic and random). θ_e and θ_d are the angular half-light radii for the elliptical and disk model host, respectively, in arcseconds. $\Delta\theta$ is the estimated error in the angular half-light radius in arcseconds. χ^2_e/dof and χ^2_d/dof are the reduced χ^2 values for the elliptical and disk model fits, respectively. AR_e and AR_d are the axial ratios of the hosts for the elliptical and disk models, respectively. PA_e and PA_d are the position angles of the major axis, in degrees, for the elliptical and disk models, respectively.

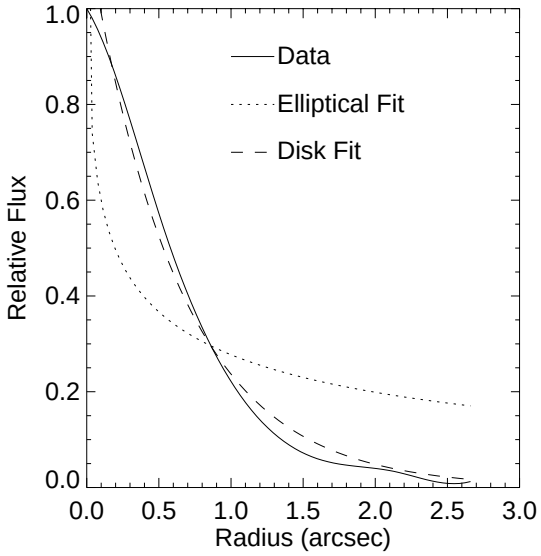

Figure 5. The one-dimensional radial profile of the SDSS 2324+0021 host galaxy (after subtraction of the best fit two-dimensional modeled quasar point source) is plotted as the solid line. The one-dimensional elliptical galaxy and exponential disk profile fits are denoted by the dotted and dashed lines, respectively.

also modeled the galaxy using the PSF star directly, rather than the synthesized PSF. Using the PSF star for the modeling made little difference to the flux and indicates that PSF mismatch errors have little influence on the magnitude estimate for the quasar host in these cases, probably because most of the flux of the host galaxy is outside the core of the PSF.

6.2. Galaxy Magnitudes and Black Hole Masses

Black hole masses were estimated from the galaxy luminosities using the empirical relationship of van der Marel,[35] adjusted to $H_0 = 70$ km/s/Mpc. We also assumed a cosmology of $\Omega_\Lambda = 0.7$ and $\Omega_M = 0.3$ when calculating the intrinsic properties of the quasars.

To obtain the galaxy absolute magnitudes we estimated the K-corrections from the observed H-band to the rest frame V-band magnitude, assuming the galaxies formed at high redshift, $z \sim 5$. We used the galaxy models of Fioc and Rocca-Volmerange[36] to make the K-corrections, assuming a spiral model for SDSS 2324+0021 host and elliptical model for SDSS 0244+0028 host. The passive evolution of the stellar luminosity of the host galaxy[36]

Table 6. Derived Quasar Host Properties

Quasar	M_V	$r_{1/2}$ (kpc)	M_{BH}(Host) ($M_\odot$)	M_{BH}(BLR) ($M_\odot$)
SDSS 2324+0021	-20.9 ± 0.1	3.8 ± 0.8	$< 2.3\text{x}10^8$	$7.0\text{x}10^7$
SDSS 0244+0028	-22.7 ± 0.1	22 ± 11	$1.3\text{x}10^9$	$3.4\text{x}10^8$

Notes: $r_{1/2}$ is the half-light radius. M_{BH}(Host) is the black hole mass estimated from the host galaxy luminosity. M_{BH}(BLR) is the black hole mass estimated using the width of the Mg II emission line.

was also estimated in order to relate the host galaxies at $z \sim 1$ to those in the local universe, on which the black hole mass–bulge luminosity correlation is calibrated.

We also estimated black hole masses from the FWHM of the Mg II emission line[37] for comparison to the galaxy luminosity black hole masses. Host galaxy absolute magnitudes and black hole mass estimates are listed in Table 6.

7. DISCUSSION

The SDSS 2324+0021 host is one of the lower redshift quasars in our sample, so it is unsurprising that it was easily detected with relatively short total integration time.

The SDSS 0244+0028 host was comfortably detected, but residual PSF error is apparent. However, the outer regions of the galaxy dominate the galaxy luminosity and small errors within the core fitting region will have little effect on the total galaxy magnitude. The image clearly shows two probable companion galaxies, 3.″3 to the west and 3.″6 to the northwest, though there is no clear indication of interaction.

The LGS AO observations have proved effective at detecting hosts around $z < 1$ quasars. The accuracy of the PSFs most limits the accuracy of the galaxy host luminosity measurements. However, for these lower redshift quasars the errors are not large enough to prevent us from obtaining scientifically useful results. It will be necessary to make better PSF calibration if we wish to study much brighter quasars relative to their hosts or quasars at significantly higher redshift. This may involve more frequent PSF observations, better matching of the PSF star–PGS to the quasar–QGS pair, or a different approach, such as PSF reconstruction from WFS telemetry information, such as Veran[38] has suggested.

Scale sizes and magnitudes of the quasar hosts are comparable to the nine $z \sim 1$ quasar hosts from the HST/NICMOS study by Kukula et al.,[9] as shown in Figure 6. Our hosts (both NGS[11] and LGS observed) are, in general, a little fainter and closer to the predictions of Kauffmann and Haehnelt[39] concerning the correlation between host magnitude and quasar magnitude. Our observed sample is thus far too small to make any definitive finding, but a larger sample will show if this trend continues. If this trend continues in the larger sample, it may be as a result of the SDSS quasar survey having fewer selection biases than typical optical surveys. Previous optical surveys tended to select very blue quasars, which are sensitive to small amounts of reddening in the host. These surveys would be expected to favor quasars in less dusty hosts, i.e. giant ellipticals.

Comparing the black hole mass estimates show that for both SDSS 2324+0021 and SDSS 0244+0028 the black hole mass estimated from the galaxy luminosity is about a factor of 3.5 higher than the black hole mass estimated from the Mg II line width. The black hole mass estimated from the host luminosity for SDSS 2324+0021 is an upper limit because the spiral model includes the disk emission and the host luminosity–black hole mass correlation is valid only for the bulge luminosity. SDSS 0244+0028 has nearby galaxies in the field, so there is the possibility of interactions. The most discrepant black hole mass estimates in Dunlop et al.,[40] who examined $z \sim 0.2$ quasar hosts with HST and made similar black hole mass estimates, were in galaxies showing interactions. Perhaps the bulge mass–luminosity estimates in interacting systems are too high. Possible reasons for this include a starburst in the merger system, the merger of the black holes of the two galaxies and the subsequent accretion

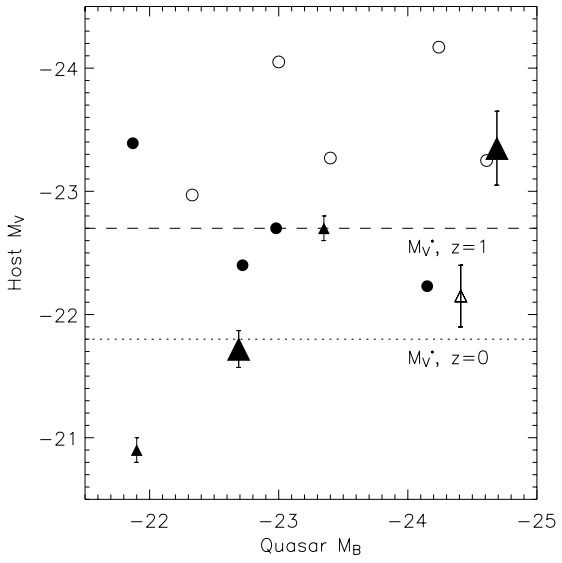

Figure 6. Host M_V plotted against quasar M_B. Our points are shown as triangles, with the large triangles denoting the quasars analyzed for this paper; the points of Kukula et al.[9] are indicated by circles. Filled symbols denote radio-quiet quasars and open symbols radio-loud quasars. The dotted line indicates the magnitude of an L^* galaxy at $z = 0$, the dashed line is the same galaxy at $z = 1$, assuming passive evolution of a stellar population formed at $z \sim 5$.

of significant amounts of matter into the black hole. Large differences between black hole mass estimates derived from emission-line widths and host bulge luminosities may thus be indicators of a quasar formed from a recent merger event.

The advent of large samples of quasar from the SDSS and Anglo-Australian 2dF surveys means that significant numbers of quasars near sufficiently bright stars for tip-tilt correction have become available. The image quality achieved with LGS AO correction has proven that scientifically interesting results can be obtained. Thus we expect to be able to form statistically useful samples of high-quality quasar host images in the near future.

ACKNOWLEGMENTS

We thank Don Gavel for valuable support and the AO group at Lawrence Livermore National Laboratory (LLNL) as a whole for their hard work on the AO system over the years. This work was partly carried out at the Jet Propulsion Laboratory, California Institute of Technology, under contract with the National Aeronautics and Space Administration (NASA). The Guide Star Catalog was produced at the Space Telescope Science Institude under government grant.

REFERENCES

1. J. Kristian, "Quasars as events in the nuclei of galaxies: The evidence from direct photographs," *Astrophys. J.* **179**, pp. L61–L65, 1973.
2. J. B. Hutchings, B. Campbell, C. Pritchet, and D. Crampton, "Optical morphology of 13 QSOs," *Astrophys. J.* **247**, pp. 743–749, 1981.
3. S. Wyckoff, P. A. Wehinger, and T. Gehren, "Resolution of quasar images," *Astrophys. J.* **247**, pp. 750–761, 1981.
4. E. P. Smith, T. M. Heckman, G. D. Bothun, W. Romanishin, and B. Balick, "On the nature of QSO host galaxies," *Astrophys. J.* **306**, pp. 64–89, 1986.

5. M. J. Disney, P. J. Boyce, J. C. Blades, A. Boksenberg, P. Cane, J. M. Deharveng, F. Macchetto, C. D. Mackay, W. B. Sparks, and S. Phillipps, "Interacting elliptical galaxies as hosts of intermediate redshift quasars," *Nature* **376**, p. 150, 1995.
6. J. N. Bahcall, S. Kirhakos, D. H. Saxe, and D. P. Schnieder, "Hubble Space Telescope images of a sample of 20 nearby luminous quasars," *Astrophys. J.* **479**, pp. 642–658, 1997.
7. J. S. Dunlop, G. L. Taylor, D. H. Hughes, and E. I. Robson, "Infrared imaging of the host galaxies of radio-loud and radio-quiet quasars," *Mon. Not. Roy. Astron. Soc.* **264**, pp. 455–488, 1993.
8. S. E. Ridgway, T. M. Heckman, D. Calzetti, and M. Lehnert, "NICMOS imaging of the host galaxies of $z \sim 2-3$ radio-quiet quasars," *Astrophys. J.* **550**, pp. 122–141, 2001.
9. M. J. Kukula, J. S. Dunlop, R. J. McLure, L. Miller, W. J. Percival, S. A. Baum, and C. P. O'Dea, "A NICMOS imaging study of high-z quasar host galaxies," *Mon. Not. Roy. Astron. Soc.* **326**, pp. 1533–1546, 2001.
10. A. Stockton, G. Canalizo, and L. M. Close, "PG 1700+518 revisited: Adaptive-optics imaging and a revised starburst age for the companion," *Astrophys. J.* **500**, pp. L121–L127, 1998.
11. M. Lacy, E. L. Gates, S. E. Ridgway, W. de Vries, G. Canalizo, J. P. Lloyd, and J. R. Graham, "Observations of quasar hosts with adaptive optics at Lick Observatory," *Astron. J.* **124**, pp. 3023–3030, 2002.
12. S. M. Croom, D. Schade, B. J. Boyle, T. Shanks, L. Miller, and R. J. Smith, "Gemini imaging of QSO host galaxies at $z \sim 2$." Astrophys. J., in press (astro-ph/0401442), 2004.
13. A. Stockton and J. W. MacKenty, "3CR249.1 and Ton202 - Luminous QSOs in interacting systems," *Nature* **305**, pp. 678–682, 1983.
14. A. Laor, "On quasar masses and quasar host galaxies," *Astrophys. J.* **505**, pp. L83–L86, 1998.
15. A. Wandel, "Black holes of active and quiescent galaxies. I. The black hole-bulge relation revisited," *Astrophys. J.* **565**, pp. 762–772, 2002.
16. R. J. McLure, M. J. Kukula, J. S. Dunlop, S. A. Baum, C. P. O'Dea, and D. H. Hughes, "A comparative HST imaging study of the host galaxies of the radio-quiet quasar, radio-loud quasars and radio galaxies - I," *Mon. Not. Roy. Astron. Soc.* **308**, pp. 377–404, 1999.
17. A. Laor, "On black hole masses and radio loudness in active galactic nuclei," *Astrophys. J.* **543**, pp. L111–L114, 2000.
18. M. Lacy, S. A. Laurent-Muehleisen, S. E. Ridgway, R. H. Becker, and R. L. White, "The radio luminosity-black hole mass correlation for quasars from the FIRST bright quasar survey and a "unification scheme" for radio-loud and radio-quiet quasars," *Astrophys. J.* **551**, pp. L17–L21, 2001.
19. T. A. Boroson, "Black hole mass and Eddington ratio as drivers for the observable properties of radio-loud and radio-quiet QSOs," *Astrophys. J.* **565**, pp. 78–85, 2002.
20. J.-H. Woo and C. M. Urry, "The independence of active galactic nucleus black hole mass and radio loudness," *Astrophys. J.* **581**, pp. L5–L7, 2002.
21. G. Kauffman, T. M. Heckmanand, C. Tremonti, J. Brinchmann, S. Charlot, S. D. M. White, S. E. Ridgway, J. Brinkman, M. Fukugita, P. B. Hall, Z. Ivezic, G. T. Richards, and D. P. Schneider, "The host galaxies of active galactic nuclei," *Mon. Not. Roy. Astron. Soc.* **346**, pp. 1055–1077, 2003.
22. X. Fan, "Simulation of stellar objects in SDSS color space," *Astron. J.* **117**, pp. 2528–2551, 1999.
23. G. T. Richards, X. Fan, D. P. Schneider, D. E. V. Berk, M. A. Strauss, D. G. Yor, J. E. Anderson Jr., S. F. Anderson, J. Annis, N. A. Bahcall, M. Bernardi, J. W. Briggs, J. Brinkmann, R. Brunner, S. Burles, L. Carey, F. J. Castander, A. J. Connolly, J. H. Crocker, I. Csabai, M. Doi, D. Finkbeiner, S. D. F. ad J. A. Frieman, M. Fukugita, J. E. Gunn, R. B. Hindsley, Z. Ivezic, S. Kent, G. R. Knapp, D. Q. Lamb, R. F. Leger, D. C. Long, J. Loveday, R. H. Lupton, T. A. McKay, A. Meiksin, A. Merrelli, J. A. Munn, H. J. Newberg, M. Newcomb, R. C. Nichol, R. Owen, J. R. Pier, A. Pope, M. W. Richmond, C. M. Rockosi, D. J. Schlegel, W. A. Siegmund, S. Smee, Y. Snir, C. Stoughton, C. Stubbs, M. SubbaRao, S. A. Szalay, G. P. Szokoly, C. Tremonti, A. Uomoto, P. Waddell, B. Yanny, and W. Zheng, "Colors of 2625 quasars at $0 < z < 5$ measured in the Sloan Digital Sky Survey photometric system," *Astron. J.* **121**, pp. 2308–2330, 2001.

24. B. J. Bauman, D. T. Gavel, K. E. Waltjen, G. J. F. ad K. A. Keahi, T. C. Kuklo, S. K. Lopes, M. J. Newman, and S. S. Olivier, "New optical design of adaptive optics system at Lick Observatory," *Proc. SPIE* **3762**, pp. 194–200, 1999.
25. B. J. B. ad D. T. Gavel, K. E. Waltjen, G. J. Freeze, R. L. Hurd, E. L. Gates, C. E. Max, S. S. Olivier, and D. M. Pennington, "Update on optical design of adaptive optics system at Lick Observatory," *Proc. SPIE* **4494**, pp. 19–29, 2002.
26. D. T. Gavel, S. S. Olivier, B. J. Bauman, C. E. Max, and B. A. Macintosh, "Progress with the Lick adaptive optics system," *Proc. SPIE* **4007**, pp. 63–70, 2000.
27. D. T. Gavel, C. E. Max, S. S. Olivier, B. J. Bauman, D. M. Pennington, B. A. Macintosh, J. Patience, C. G. Brown, P. M. Danforth, R. L. Hurd, E. L. Gates, S. A. Severson, and J. P. Lloyd, "Science with laser guide stars at Lick Observatory," *Proc. SPIE* **4494**, pp. 336–342, 2002.
28. D. T. Gavel, E. L. Gates, C. E. Max, S. S. Olivier, B. J. Bauman, D. M. Pennington, B. A. Macintosh, J. Patience, C. G. Brown, P. M. Danforth, R. L. Hurd, S. A. Severson, and J. P. Lloyd, "Recent science and engineering results with the laser guidestar adaptive optic system at Lick Observatory," *Proc. SPIE* **4839**, pp. 354–359, 2003.
29. J. P. Lloyd, M. C. Liu, B. A. Macintosh, S. A. Severson, W. T. Deich, and J. R. Graham, "IRCAL: the infrared camera for adaptive optics at Lick Observatory," *Proc. SPIE* **4008**, pp. 814–821, 2000.
30. M. D. Perrin, J. R. G. ad P. Kalas, J. P. Lloyd, C. E. Max, D. T. Gavel, D. M. Pennington, and E. L. Gates, "Laser guide star adaptive opitcs imaging polarimetry of Herbig Ae/Be stars," *Science* **33**, pp. 1345–1348, 2004.
31. D. P. Schneider, X. Fan, P. B. Hall, S. Jester, G. T. Richards, C. Stoughton, M. A. Strauss, M. SubbaRao, D. E. V. Berk, S. F. Anderson, W. N. Brandt, J. E. Gunn, J. Gray, J. R. Trump, W. Voges, B. Yanny, N. A. Bahcall, M. R. Blanton, W. N. Boroski, J. Brinkmann, R. Brunner, S. Burles, F. J. Castander, M. Doi, D. Eisenstein, J. A. Frieman, M. Fukugita, T. M. Heckmann, G. S. Hennessy, Z. Ivezic, S. Kent, G. R. Knapp, D. Q. Lamb, B. C. Lee, J. Loveday, R. H. Lupton, B. Margon, A. Meiksin, J. A. Munn, H. J. Newberg, R. C. Nichol, M. Niederste-Ostholt, J. R. Pier, M. W. Richmond, C. M. Rockosi, D. H. Saxe, D. J. Schlegel, A. S. Szalay, A. R. Thakar, A. Uomoto, and D. G. York, "The Sloan Digital Sky Survey quasar catalog. II. First data release," *Astron. J.* **126**, pp. 2579–2593, 2003.
32. S. E. Persson, D. C. Murphy, W. Krzeminski, M. Roth, and M. J. Rieke, "A new system of faint near-infrared standard stars," *Astron. J.* **116**, pp. 2475–2488, 1998.
33. E. Stienbring, S. M. Faber, S. Hinkley, B. A. Macintosh, D. Gavel, E. L. Gates, J. C. Christou, M. L. Louarn, L. M. Raschke, S. A. Severson, F. Rigaut, D. Crampton, J. P. Lloyd, and J. R. Graham, "Characterizing the adaptive optics off-axis point-spread function. I. A semiempirical method for use in natural guide star observations," *Pub. Astron. Soc. Pacific* **114**, pp. 1267–1280, 2002.
34. R. J. McLure, J. S. Dunlop, and M. J. Kukula, "Two-dimensional modelling of optical Hubble Space Telescope and infrared tip-tilt images of quasar host galaxies," *Mon. Not. Roy. Astron. Soc.* **318**, pp. 693–702, 2000.
35. R. P. van der Marel, "The black hole mass distribution in early-type galaxies: Cusps in Hubble Space Telescope photometry interpreted through adiabatic black hole growth," *Astron. J.* **117**, pp. 744–763, 1999.
36. M. Fioc and B. Rocca-Volmerange, "PEGASE: a UV to NIR spectral evolution model of galaxies. Application to the calibration of bright galaxy counts," *Astron. & Astrophys.* **326**, pp. 950–962, 1997.
37. R. J. McLure and M. J. Jarvis, "Measuring the black hole masses of high redshift quasars," *Mon. Not. Roy. Astron. Soc.* **337**, pp. 109–116, 2002.
38. J.-P. Véran, F. Rigault, H. Maître, and D. Rouan, "Estimation of the adaptive optics long-exposure point-spread function using control loop data," *J. Opt. Soc. Am. A* **14**, pp. 3057–3062, 1997.
39. G. Kauffmann and M. Haehnelt, "A unified model for the evolution of galaxies and quasars," *Mon. Not. Roy. Astron. Soc.* **311**, pp. 576–588, 2000.
40. J. S. Dunlop, R. J. McLure, M. J. Kukula, S. A. Baum, C. P. O'Dea, and D. H. Hughes, "Quasars, their host galaxies and their central black holes," *Mon. Not. Roy. Astron. Soc.* **340**, pp. 1095–1135, 2003.